Journal of Zhejiang University-SCIENCE C (Computers & Electronics)
ISSN 1869-1951 (Print); ISSN 1869-196X (Online)
www.zju.edu.cn/jzus; www.springerlink.com
E-mail: jzus@zju.edu.cn

Spectrum sensing using multiple dual polarization antennas for cognitive radio systems in microcell environments*#

Yi-hu XU, Myoung-Seob LIM‡

(*Division of Electronics & Information Engineering, Chonbuk National University, Jeonju 561756, Korea*)

E-mail: {xuyh, mslim}@jbnu.ac.kr

Received Apr. 15, 2013; Revision accepted June 28, 2013; Crosschecked Sept. 16, 2013

Abstract: Spectrum sensing with multiple antennas for cognitive radio systems in microcell environments is affected by the spatial correlation among multiple antennas. To reduce the adverse effects of the spatial correlation on the spectrum sensing performance, we employ multiple dual polarization antennas at the sensing node of secondary users. The analysis of the spatial correlation is derived using the propagation characteristics of the electromagnetic wave based on the scattering patch model in a multipath microcell environment. The superiority of spectrum sensing with multiple dual polarized antennas over multiple mono-polarized antennas is shown by analyzing the false alarm and detection probabilities with the correlation among the antennas in a microcell environment.

Key words: Dual polarization, Multiple antennas, Spatial correlation, Spectrum sensing, Cognitive radio
doi:10.1631/jzus.C1300086 **Document code:** A **CLC number:** TN92

1 Introduction

The multitude of different wireless devices and radio access technologies, the dramatic increase in the number of wireless subscribers, and the continuous demand for higher data rates are all reasons that the radio frequency spectrum has become increasingly crowded. However, measurements performed by the Federal Communication Commission (FCC) indicated that wide ranges of the radio spectrum are rarely used most of the time, while other frequency bands are heavily utilized (FCC, 2002). The recently proposed concept of cognitive radio (CR) solves the inefficient spectrum utilization problem by allowing users to opportunistically access the unused primary spectrum without causing harmful interference to primary users (Mitola, 1999; 2000). Spectrum sensing as a key technique for CR has been researched actively (Akyildiz *et al*., 2006).

Multiple antennas offer space diversity and can improve spectrum sensing performance (Kuppusamy and Mahapatra, 2008; Lee *et al*., 2008). In fact, the use of multiple antenna techniques in CR is one approach for spectrum sensing by exploiting the available spatial domain observations. However, in those previous works, the adverse effects of the antenna correlation on the sensing performance were not analyzed.

In CR networks, the great distance between the primary user and the secondary user (greater than 100 km in IEEE 802.22 WRAN systems) generates a small angular spread at the sensing node of the secondary user (IEEE 802.22 Working Group on Wireless Regional Area Networks, 2011). It is therefore inevitable that there is a high degree of correlation among the antennas at the sensing node. To analyze the spectrum sensing performance with multiple antennas in IEEE 802.22 WRAN-based CR systems, the effect of the antenna correlation needs to be

‡ Corresponding author

* Project supported by the Brain Korea 21 Plus of Korea and the Ministry of Trade, Industry & Energy (MOTIE) and IDEC Platform Center (IPC) for Smart Car of Korea

A preliminary version was presented at the 18th Asia-Pacific Conference on Communications, October 15–17, 2012, Jeju Island, Korea

investigated. In Kim *et al*. (2009), the detection and false alarm probabilities for energy detectors in CR were derived for cases in which there is a correlation among multiple antennas of the sensing node of the secondary user.

In our previous work (Xu and Lim, 2012), to reduce the adverse effect of the spatial correlation on the spectrum sensing performance, we proposed to employ multiple dual polarization antennas, with both vertical and horizontal polarization antennas at the sensing node of the secondary user. To describe the spatial correlation between antennas in a simple way, we focused our work on the line-of-sight (LOS) channel as a propagation environment. In a practical wireless communication channel, however, the propagation situation may be very complex.

As an extension of the previous work, to obtain a more realistic spectrum sensing performance, the microcell environment is considered in the present study to be a multipath channel environment. All of the analysis and the derivation of the corresponding equations are based on the multipath channel environment. Through the simulation results of the spatial correlation, we also analyze the spatial correlation when the distance and the angle between the multiple antennas are changing. Considering the spatial correlation among antennas, to protect the primary user, the spectrum sensing performance of the CR receiver with dual polarized multiple antennas is analyzed in terms of the probabilities of the detection and the false alarm, and the closed-form expressions for the probabilities of the detection and the false alarm are derived based on energy detection. By analyzing the spectrum sensing performance with multiple dual polarized antennas and comparing the spectrum sensing performance with that of multiple mono-polarized antennas, it is shown that the proposed method has fewer adverse effects due to the spatial correlation among antennas.

2 Correlation analyses for multiple dual polarized antennas in a microcell environment

In this section, we derive the spatial correlation for the multiple antennas in a CR under a multipath channel in a microcell environment. An analysis of the spatial correlation for multiple antennas shows that the correlation value is highly related to the angle and the distance between the multiple antennas. If two antennas are orthogonal to each other, the cross correlation is at the minimum.

2.1 Multipath channel environment in a microcell environment

The propagation situation of an electromagnetic wave is dependent on the scattering effect in a practical wireless communication channel such as a microcell environment (Svantesson, 2001a). To explore the spectrum sensing performance of CR under a multipath channel in a microcell environment, it is necessary to provide a more realistic model (Fig. 1). In the microcell environment, the reflector-like buildings that generate the reflected waves in several directions are simplified in the patch model as scatters.

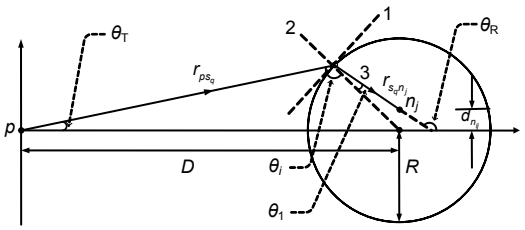

Fig. 1 Microcell channel environment

The scatters are distributed uniformly within a circle of radius R centered at the sensing node that is located at a distance D from the primary transmitter. $d_{n_{ij}}$ is the distance between the ith and jth antennas at the sensing node, r_{ps_q} is the distance from the primary user to the qth scatter, and $r_{s_q n_j}$ is the distance from the qth scatter to the jth antenna at the sensing node

2.2 Scattering patch model in a microcell environment

The propagation characteristics of the plane electromagnetic wave can be described geometrically using the scattering patch model shown in Fig. 2.

To solve for θ_i, θ_s, and ϕ_s, we link the microcell model with the scattering patch model (Liu and Zhang, 2008). k_s, k_{ss}, and k_{sss} are the slopes of lines 1, 2, and 3, respectively (Fig. 1). We set o and s as the position of the scatter and the receiver, respectively. l_1, l_2, l_3, and l_4 are the distances as marked in Fig. 2.

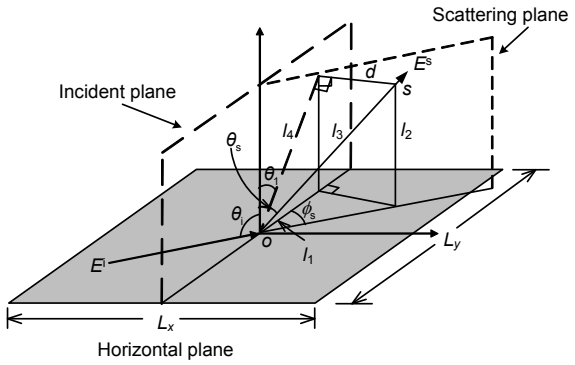

Fig. 2 Scattering patch model

θ_i is the angle of the incident wave, and θ_s and ϕ_s are the elevation and azimuth angles of the scattering wave orientation, respectively

From Fig. 2, we have

$$k_{ss} = y_s / (x_s - D), \tag{1}$$

$$k_s = -1 / k_{ss}, \tag{2}$$

$$k_{sss} = (y_s - y_{rp}) / (x_s - x_{rp}), \tag{3}$$

$$\theta_R = \arccos(k_{sss}), \tag{4}$$

$$\theta_1 = \theta_R - \arctan(k_{ss}), \tag{5}$$

$$\theta_T = \arctan[(y_s - y_{tp}) / (x_s - x_{tp})], \tag{6}$$

$$\theta_i = \arctan(k_{ss}) - \theta_T, \tag{7}$$

$$l_4 = \sqrt{(x_s - x_{tp})^2 + (y_s - y_{tp})^2}, \tag{8}$$

$$l_1 = l_4 \sin\theta_1, \tag{9}$$

$$l_2 = l_4 \cos\theta_1, \tag{10}$$

$$l_3 = \sqrt{l_4^2 + d^2}, \tag{11}$$

$$\theta_s = \arccos(l_2 / l_3), \tag{12}$$

$$\varphi_s = \arctan(d / l_1). \tag{13}$$

Herein x_s and y_s are the abscissa and ordinate location points of the scatter, respectively; x_{tp} and y_{tp} are the abscissa and ordinate location points of the transmitter, respectively; x_{rp} and y_{rp} are the abscissa and ordinate location points of the receiver, respectively; θ_R and θ_T are the angle of arrival (AOA) and the angle of departure (AOD), respectively.

2.3 Scattering matrix

The incident and scattered waves are related to the scattering matrix, $\boldsymbol{S}$ (Tarng and Ju, 1999). The scattering matrix $\boldsymbol{S}$ is derived from the θ_i, θ_s, and ϕ_s as depicted geometrically in Fig. 2.

The scattering matrix element S_{jq}, which represents the scattering characteristic between the jth parallel polarization antenna and the qth scatter, is defined by the radar cross section (RCS) σ_{jq}:

$$S_{jq}(\alpha,\beta) = \frac{\sqrt{\sigma_{jq}(\alpha,\beta)}}{\sqrt{4\pi} r_{s_q n_j}}, \tag{14}$$

where α, β=1 or 2. The indexes α and β denote the number of elements in the scattering matrix.

For each scattering patch, L_x and L_y are the widths of the two borders of the scatter (Fig. 2). The RCS, σ_{jq} (Ruck *et al*., 1970), which defines the relationship between the scattered energy and the incident energy, is defined as follows:

$$\sigma_{jq}(\alpha,\beta) = \frac{\beta^2}{\pi}(L_x L_y)^2 \left(\frac{\sin(\beta\xi_x L_x/2)}{\beta\xi_x L_x/2}\right)^2 \cdot \left(\frac{\sin(\beta\xi_y L_y/2)}{\beta\xi_y L_y/2}\right)^2 \left|\gamma_{\alpha\beta}\right|^2, \tag{15}$$

where

$$\xi_x = \sin\theta_i - \sin\theta_s \sin\varphi_s,\ \xi_y = \sin\theta_s \sin\varphi, \tag{16}$$

$$\begin{cases} \gamma_{11} = \cos\theta_i \cos\varphi_s \Gamma_\perp(\theta_i), \\ \gamma_{12} = \sin\varphi_s \Gamma_\parallel(\theta_i), \\ \gamma_{21} = \cos\theta_i \cos\varphi_s \sin\varphi_s \Gamma_\perp(\theta_i), \\ \gamma_{22} = -\cos\theta_i \cos\varphi_s \Gamma_\parallel(\theta_i). \end{cases} \tag{17}$$

$\Gamma_\perp(\theta_i)$ and $\Gamma_\parallel(\theta_i)$ are the Fresnel reflection coefficients of the patch for the polarizations perpendicular and parallel to the incident plane, respectively (Tarng *et al*., 1997).

2.4 Characteristics of spatial correlation in a microcell environment

The microcell environment shown in Fig. 1 is based on electromagnetic wave scattering. The primary user transmits an electromagnetic wave along the $\boldsymbol{r}_{ps}$ direction. After some time, this transmitted wave reaches the scatter and gives rise to a scattered wave. Later, the scattered wave impinges on the antennas at the sensing node from the $\boldsymbol{r}_{sn}$ direction and induces a voltage. To reduce the complexity of the model, the interaction between the scatters is neglected. However, some of the properties of multiple

scattering are retained by placing a scattering object at the last and/or first reflection (Svantesson, 2001b).

For the qth scatter, it is possible to express the transmitted field at point $\boldsymbol{r}_{ps_q}$, with the antenna positioned at the primary user, in the form

$$\boldsymbol{E}_{\mathrm{t}}(\boldsymbol{r}_{ps_q})=\frac{\exp\left[\mathrm{j}\left(\omega t-k\left|\boldsymbol{r}_{ps_q}\right|\right)\right]}{\left|\boldsymbol{r}_{ps_q}\right|}G_{\mathrm{t}}\left(\boldsymbol{r}_{ps_q}\right)\boldsymbol{g}_{\mathrm{t}}\left(\boldsymbol{r}_{ps_q}\right), \quad (18)$$

where G_{t} is the element pattern of the transmitted field, $\boldsymbol{g}_{\mathrm{t}}$ is the orientation of the transmitted field, k is the wave number, defined as $2\pi/\lambda$, and ω is the angular frequency of the electromagnetic wave signal.

For a z-oriented dipole antenna of length l, G_{t} and $\boldsymbol{g}_{\mathrm{t}}$ can be expressed as

$$G_{\mathrm{t}}=\frac{\mathrm{j}\eta I_0}{2\pi}\left[\cos\left(\frac{kl}{2}\cos\theta\right)-\cos\left(\frac{kl}{2}\right)\right]\Big/\sin\theta, \quad (19)$$

$$\boldsymbol{g}_{\mathrm{t}}=\boldsymbol{x}\cos\theta\cos\varphi+\boldsymbol{y}\cos\theta\sin\varphi-\boldsymbol{z}\sin\theta, \quad (20)$$

where $\boldsymbol{x}$, $\boldsymbol{y}$, $\boldsymbol{z}$ are the basis vectors in the rectangular coordinate system, η is the intrinsic impedance of the medium, and I_0 is the input current.

After some time, the transmitted wave will be scattered by the scatter. Due to the scattering effect, a new field $\boldsymbol{E}_{\mathrm{s}}$ is radiated and received at the sensing node. The field at the jth antenna on the sensing node can be expressed as

$$\boldsymbol{E}_{\mathrm{s}}(\boldsymbol{r}_{s_qn_j})=\frac{\exp\left[\mathrm{j}\left(\omega t-k\left|\boldsymbol{r}_{s_qn_j}\right|\right)\right]}{\left|\boldsymbol{r}_{s_qn_j}\right|}\left|\boldsymbol{E}_{\mathrm{t}}\right|S_{jq}\boldsymbol{g}_{\mathrm{t}}\left(\boldsymbol{r}_{ps_q}\right), \quad (21)$$

where $\left|\boldsymbol{E}_{\mathrm{t}}\right|$ is the amplitude of the field incident upon the scatter.

From the derived scattered field $\boldsymbol{E}_{\mathrm{s}}$, the received field at the jth antenna of the sensing node due to the qth scatter can be obtained as

$$\boldsymbol{E}_{\mathrm{r}}(\boldsymbol{r}_{s_qn_j})=G_{\mathrm{r}}\left(-\boldsymbol{r}_{s_qn_j}\right)\boldsymbol{g}_{\mathrm{r}}\left(-\boldsymbol{r}_{s_qn_j}\right)\cdot\boldsymbol{E}_{\mathrm{s}}, \quad (22)$$

where G_{r} and $\boldsymbol{g}_{\mathrm{r}}$ are the element pattern and orientation of the received field, respectively.

Using the above results, the total received field at the jth antenna is obtained as follows:

$$E_{\mathrm{total},n_j}=\sum_{q=1}^{N_{\mathrm{s}}}\left\{\exp\left\{\mathrm{j}\left[\omega t-k\left(\left|\boldsymbol{r}_{ps_q}\right|+\left|\boldsymbol{r}_{s_qn_j}\right|\right)\right]\right\}\Big/\left(\left|\boldsymbol{r}_{ps_q}\right|\left|\boldsymbol{r}_{s_qn_j}\right|\right)\cdot G_{\mathrm{t}}\left(\boldsymbol{r}_{ps_q}\right)G_{\mathrm{r}}\left(-\boldsymbol{r}_{s_qn_j}\right)\boldsymbol{g}_{\mathrm{r}}\left(-\boldsymbol{r}_{s_qn_j}\right)\boldsymbol{S}\boldsymbol{g}_{\mathrm{t}}\left(\boldsymbol{r}_{ps_q}\right)\right\}, \quad (23)$$

where N_{s} is the total number of scatters.

Note that in Eq. (23) the antenna scalar C is omitted, to reduce notational complexity.

The correlation between the ith and jth antennas can be expressed as (Raoof and Prayongpun, 2005)

$$\rho_{ij}=\frac{E^2\left(E_{\mathrm{total},n_i}E^*_{\mathrm{total},n_j}\right)}{E\left(\left|E_{\mathrm{total},n_i}\right|^2\right)E\left(\left|E_{\mathrm{total},n_j}\right|^2\right)}. \quad (24)$$

The antenna correlation matrix $\boldsymbol{R}$ is an $N_{\mathrm{a}}\times N_{\mathrm{a}}$ matrix, the components of which are defined as

$$R_{ij}=\begin{cases}\rho_{ij}, & i\le j,\\ R^*_{ji}, & i>j,\end{cases} \quad (25)$$

where $j=1, 2, \ldots, N_{\mathrm{a}}$, $0\le\rho_{ij}\le1$. N_{a} is the total number of antennas at the sensing node, and λ_j is the jth eigenvalue of the antenna correlation matrix $\boldsymbol{R}$.

Fig. 3 shows the cross-correlation simulation results between the two antennas. Assuming that there

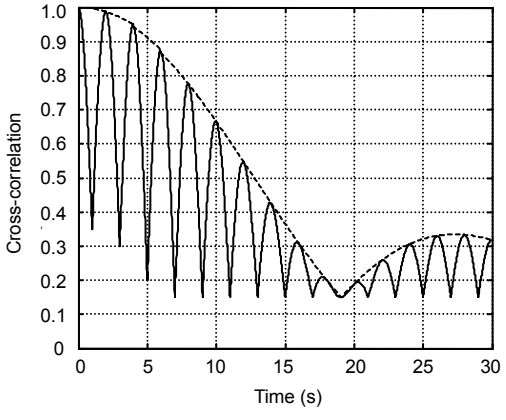

Fig. 3 Cross-correlation simulation results between two antennas

One of the dipole antennas rotates around its phase center with a constant angular speed of $\pi/2$ rad/s, and moves with a constant linear speed of 5 mm/s. The dotted line shows the correlation between antennas when the angle between the antennas is fixed and the distance between the antennas increases; the solid line shows the correlation between antennas when the angle between the antennas varies linearly and the distance between the antennas increases

are two dipole antennas, one of the dipole antennas rotates around its phase center with a constant angular speed of π/2 rad/s, and moves with a constant linear speed of 5 mm/s. From the figure, it is easy to see that if two antennas are orthogonal to each other, which means that the angle between the two antennas is $\theta_p=\pi/2+p\pi$ (p=0, 1, …), the cross-correlation reaches the minimum value. Thus, we propose the application of dual polarized multiple antennas for the spectrum sensing to reduce the adverse effect of the correlation.

3 Spectrum sensing performance of multiple dual polarized antennas in a multipath channel environment

In this section, we derive the false alarm and the detection probabilities of spectrum sensing with multiple antennas in CR under a multipath channel environment where there is a correlation among the multiple antennas of the sensing node. The spectrum sensing performance of multiple dual polarized antennas is compared with that of multiple mono-polarized antennas in a multipath channel environment.

Defining $x_j(m)$ as the induced voltage signal at the mth sampling time from the jth antenna at which the scattered electromagnetic wave was received, the $MN_a\times1$ received signal matrix $\boldsymbol{X}$ at N_a antennas for M time samples is expressed as

$$\begin{aligned}\boldsymbol{X}=\big[&x_1(1),...,x_{N_a}(1),x_1(2),...,x_{N_a}(2),...,\\&x_1(M),...,x_{N_a-1}(M),x_{N_a}(M)\big]^{\mathrm{T}}.\end{aligned}\tag{26}$$

By summing all of the received signal energies at the sensing node with multiple antennas, the test statistic for the energy detector can be expressed as (Kay, 1998)

$$T_e(\boldsymbol{X})=\boldsymbol{X}^{\mathrm{H}}\boldsymbol{X}=\sum_{m=1}^{M}\sum_{j=1}^{N_a}\left|x_j(m)\right|^2.\tag{27}$$

To derive the false alarm and detection probabilities for the spectrum sensing with the energy detector, we should derive the probability density function (PDF) of $T_e(\boldsymbol{X})$ for both hypothesis H_0 with only noise and hypothesis H_1 with noise and the received signal. Under hypothesis H_0, $x_j(m)$ has a complex Gaussian distribution with zero mean and variance σ_n^2 for all j and m values. According to the central limit theorem (CLT), the distribution of $T_e(\boldsymbol{X})$ based on the energy detector as in Eq. (27) can be expressed as follows:

Under H_0 with only noise, because of the independent and identically distributed (i.i.d.) characteristics of noise,

$$H_0:T_e(\boldsymbol{X})\sim N(MN_a\sigma_n^2,MN_a\sigma_n^4).\tag{28}$$

The CLT approximates the original PDF well in cases where the number of samples is large enough (e.g., MN_a>10 in practice) (Quan *et al*., 2008).

Under H_1 with noise and the received signal, using the moment generating function (Alouini *et al*., 2001), the distribution of the test statistics is expressed as

$$H_1:T_e(\boldsymbol{X})\sim N\left(MN_a(P\sigma_h^2+\sigma_n^2),M\sum_{j=1}^{N_a}(P\sigma_h^2\lambda_j+\sigma_n^2)^2\right),\tag{29}$$

where λ_j is the eigenvalue of the correlation matrix, obtained according to Eq. (25), and P is the average power at the sensing node. σ_n^2 is the variance of noise, and σ_h^2 is the variance of the received signal, which is dependent on the channel.

Based on the distributions of $T_e(\boldsymbol{X})$ under H_0 and H_1, the false alarm and detection probabilities for the energy detector can be obtained according to the decision rule. Using the test statistics for the energy detector in Eq. (27), the decision rule is defined by

$$T_e(\boldsymbol{X})\underset{H_0}{\overset{H_1}{\gtrless}}\tau_e,\tag{30}$$

where τ_e is the decision threshold of the energy detector.

The detection probability for spectrum sensing with multiple dual polarization antennas can be expressed as follows:

$$P_{de}=Q\left\{[\tau_e-MN_a(P\sigma_h^2+\sigma_n^2)]\Big/\sqrt{M\sum_{j=1}^{N_a}(P\sigma_h^2\lambda_j+\sigma_n^2)^2}\right\},\tag{31}$$

where $Q(x)=\int_x^{\infty} \mathrm{e}^{-t^2/2}\mathrm{d}t \Big/ \sqrt{2\pi}$ denotes the tail probability of the normal PDF.

To protect the primary users in the CR system, we need a constraint of the detection probability. While maintaining the constraint of the detection probability, the spectrum sensing performance can be analyzed according to the false alarm probability. When there is a constraint of the detection probability $P_{\mathrm{de}} \geq \alpha$, the decision threshold can be derived from Eq. (31):

$$\tau_{\mathrm{e}} = Q^{-1}(\alpha)\sqrt{M\sum_{j=1}^{N_{\mathrm{a}}}(P\sigma_{\mathrm{h}}^2\lambda_j+\sigma_{\mathrm{n}}^2)^2} + MN_{\mathrm{a}}(P\sigma_{\mathrm{h}}^2+\sigma_{\mathrm{n}}^2). \tag{32}$$

The false alarm probability for the spectrum sensing with multiple antennas is determined:

$$P_{\mathrm{fe}} = Q\left(\frac{\tau_{\mathrm{e}} - MN_{\mathrm{a}}\sigma_{\mathrm{n}}^2}{\sqrt{MN_{\mathrm{a}}\sigma_{\mathrm{n}}^4}}\right). \tag{33}$$

By substituting Eq. (32) into Eq. (33), the false alarm probability with a constraint of the detection probability can be derived as follows:

$$P_{\mathrm{fe}} = Q\left(Q^{-1}(\alpha)\sqrt{\frac{1}{N_{\mathrm{a}}}\sum_{j=1}^{N_{\mathrm{a}}}(\gamma\lambda_j+1)^2+\gamma\sqrt{MN_{\mathrm{a}}}}\right), \tag{34}$$

where $\gamma = P\sigma_{\mathrm{h}}^2/\sigma_{\mathrm{n}}^2$ is the signal-to-noise ratio (SNR) of the primary signal received at the sensing node.

Fig. 4 shows the false alarm probability of the spectrum sensing with an energy detector when there is a correlation between antennas for the condition with $d=\lambda_{\mathrm{c}}/8$, where λ_{c} is the wavelength of the carrier signal, in the microcell environment. From Fig. 4, it can be seen that the spectrum sensing performance of multiple dual polarization antennas is also degraded due to the multipath environment. However, the spectrum sensing performance with multiple dual polarization antennas is better than that with conventional multiple mono-polarized antennas in the microcell environment.

The effect of the number of antennas on the sensing performance is demonstrated in Figs. 5 and 6 for a microcell environment.

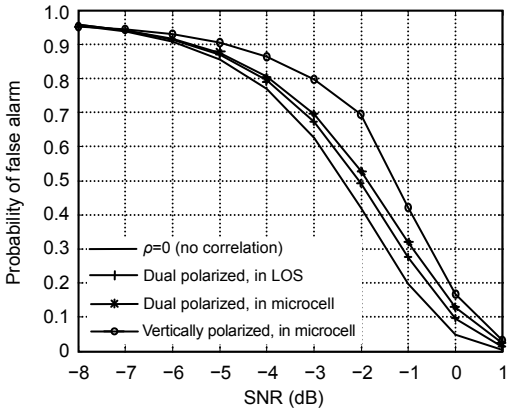

Fig. 4 Spectrum sensing performance comparison between dual polarized antennas in LOS and a microcell environment (N_{a}=2, α=0.99)

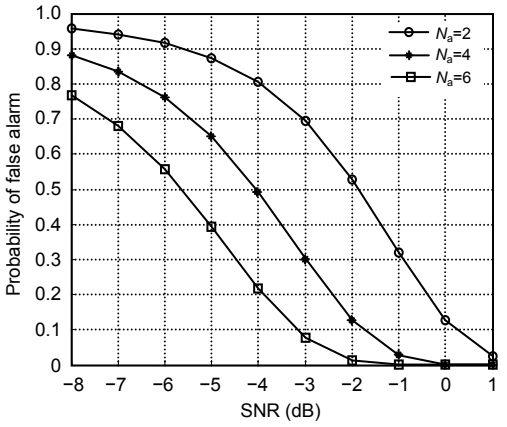

Fig. 5 Spectrum sensing performance comparison between two, four, and six dual polarized multiple antennas (α=0.99)

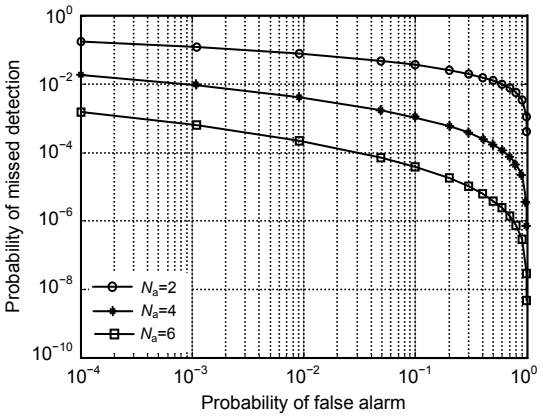

Fig. 6 The receiver operating characteristic (ROC) curves for two, four, and six dual polarized multiple antennas

Fig. 5 shows the false alarm probability of the energy detector when the multiple antennas are

linearly separated ($d=\lambda_c/8$) for $N_a=2$, 4, 6. Fig. 6 shows the complementary receiver operating characteristic (ROC) curves, i.e., the probability of missed detection ($P_m=1-P_{de}$) vs. the probability of false alarm (P_{fe}), for the dual polarized multiple antennas with various numbers of antennas in the microcell environment. For the simulations we assume that the mean SNR observed by a sensing node is 6 dB.

The simulation results in Figs. 5 and 6 show that the sensing performance improves as the number of multiple dual polarized antennas increases.

4 Conclusions

In this paper, to consider the adverse effect of antenna correlations under a multipath channel environment such as a microcell, the correlations among the antennas are derived using the patch model, which can geometrically describe the wave propagation characteristic from each scatter around the microcell. Using the derived correlation among the antennas in a microcell environment and analyzing the detection and false alarm probabilities of the spectrum sensing with multiple dual polarized antennas for CR, it was shown that the performance of spectrum sensing with multiple dual polarization antennas is better than that with conventional multiple mono-polarized antennas.

References

Akyildiz, I.F., Lee, W.Y., Vuran, M.C., Mohanty, S., 2006. Next generation/dynamic spectrum access/cognitive radio wireless networks: a survey. *Comput. Netw.*, **50**(13): 2127-2159. [doi:10.1016/j.comnet.2006.05.001]

Alouini, M.S., Abdi, A., Kaveh, M., 2001. Sum of gamma variates and performance of wireless communication systems over Nakagami-fading channels. *IEEE Trans. Veh. Technol.*, **50**(6):1471-1480. [doi:10.1109/25.966578]

FCC, 2002. Spectrum Policy Task Force Report. Proc. Federal Communication Commission, p.1-37.

IEEE 802.22 Working Group on Wireless Regional Area Networks, 2011. IEEE 802.22-2011(TM) Standard for Cognitive Wireless Regional Area Networks (RAN) for Operation in TV Bands. Available from http://grouper.ieee.org/groups/802/22/.

Kay, S.M., 1998. Fundamentals of Statistical Signal Processing, Volume II: Detection Theory. Prentice-Hall, Upper Saddle River, NJ.

Kim, S.T., Lee, J.M., Wang, H.N., Hong, D.S., 2009. Sensing performance of energy detector with correlated multiple antennas. *IEEE Signal Process. Lett.*, **16**(8):671-674. [doi:10.1109/LSP.2009.2021381]

Kuppusamy, V., Mahapatra, R., 2008. Primary User Detection in OFDM Based MIMO Cognitive Radio. 3rd Int. Conf. on Cognitive Radio Oriented Wireless Networks and Communications, p.1-5. [doi:10.1109/CROWNCOM.2008.4562561]

Lee, J.H., Baek, J.H., Hwang, S.H., 2008. Collaborative Spectrum Sensing Using Energy Detector in Multiple Antenna System. 10th Int. Conf. on Advanced Communication Technology, p.427-430. [doi:10.1109/ICACT.2008.4493794]

Liu, H.Y., Zhang, Y.R., 2008. An Outdoor Scattering Channel Model for Dual-Polarized MIMO Systems. 2nd Int. Symp. on Intelligent Information Technology Application, p.760-764. [doi:10.1109/IITA.2008.313]

Mitola, J., 1999. Cognitive radio: making software radio more personal. *IEEE Pers. Commun.*, **6**(4):13-18. [doi:10.1109/98.788210]

Mitola, J., 2000. Cognitive Radio: an Integrated Agent Architecture for Software Defined Radio. PhD Thesis, Royal Institute of Technology (KTH), Sweden.

Quan, Z., Chi, S., Sayed, A.H., 2008. Optimal linear cooperation for spectrum sensing in cognitive radio networks. *IEEE J. Sel. Topics Signal Process.*, **2**(1):28-40. [doi:10.1109/JSTSP.2007.914882]

Raoof, K., Prayongpun, N., 2005. Channel Capacity Performance for MIMO Polarized Diversity Systems. Int. Conf. on Wireless Communications, Networking and Mobile Computing, p.1-4. [doi:10.1109/WCNM.2005.1543970]

Ruck, G.T., Barrick, D.E., Stuart, W.D., Krichbaum, C.K., 1970. Radar Cross Section Handbook, Vol. II. Plenum, New York.

Svantesson, T., 2001a. Antennas and Propagation from a Signal Processing Perspective. PhD Thesis, Chalmers University of Technology, Goteborg, Sweden.

Svantesson, T., 2001b. A Physical MIMO Radio Channel Model for Multi-element Multi-polarized Antenna Systems. IEEE Vehicular Technology Conf., p.1083-1087. [doi:10.1109/VTC.2001.956941]

Tarng, J.H., Ju, K.M., 1999. A novel 3-D scattering model of 1.8-GHz radio propagation in microcellular urban environment. *IEEE Trans. Electromagn. Compat.*, **41**(2):100-106. [doi:10.1109/15.765097]

Tarng, J.H., Chang, W.R., Hsu, B.J., 1997. Three-dimensional modeling of 900-MHz and 2.44-GHz radio propagation in corridors. *IEEE Trans. Veh. Technol.*, **46**(2):519-527. [doi:10.1109/25.580790]

Xu, Y.H., Lim, M.S., 2012. Spectrum Sensing Using Dual Polarized Multiple Antennas in Cognitive Radio Systems. Asia-Pacific Conf. on Communications, p.914-917. [doi:10.1109/APCC.2012.6388241]